Patterns in natural systems

Sewalt, L.

1

Introduction

In this thesis, we study several systems with an application in nature. While these applications (phytoplankton growth, tumor spread and vegetation patterns) have little in common, the equations that describe their behavior have strikingly similar features. The models studied in this thesis all comprise two or more coupled differential equations. Differential equations in general are equations that involve not only functions and variables, but also derivatives of functions; they are equations that connect the change of a quantity to the quantity itself. When the equations include derivatives with respect to more than one variable (time, space) they are called partial differential equations. The partial differential equations studied in this thesis are of reaction-diffusion type, which implies that they describe the spread (diffusion) of some quantity over time, under the influence of some interaction (reaction) with, usually, another quantity. Say we label two quantities u and v that interact, and we measure the spread of those quantities over a line segment – a spatial domain parametrized by x – over time t. The equations that describe this may be written as

$$\begin{aligned} u_t &= u_{xx} + f(u, v), \\ v_t &= v_{xx} + g(u, v), \end{aligned} \tag{1.1}$$

where the functions f and g describe exactly how u and v react to each other and a subscript indicates taking the derivative with respect to that variable. The second derivative with respect to the spatial variable models diffusion or natural spreading of the quantities u and v in the absence of any other forces. Furthermore, say we let x be bounded by 0 and 1, and t starts at $t = 0$ and may run up to infinity. To make this system of equations well-posed for solving, we provide boundary and/or initial conditions that prescribes the behavior of the solution at $t = 0$ and at the boundaries of the domain. Also, the system may depend on

parameters. Many types of questions may be posed associated to problems like (1.1). Are there unique solutions to the system (well-posedness)? Could these solutions be periodic in space or time (existence)? Does the character of a solution change significantly under the influence of changing parameters (bifurcations)? Are solutions resilient to small changes in the environment (stability)? In this general form it is hard to answer those questions, because the functions f and g may get very complex. But even in the case that $f = av$ and $g = bu$, with a, b parameters, studying existence of solutions, their bifurcations and their stability is nontrivial.

Therefore, we need some additional information to simplify the general reaction-diffusion model. The models studied in this thesis are all of reaction-diffusion type, but there is more agreement among them. Inherent through the applications, there is a clear separation of scales in all systems. The system is therefore equipped with a special small parameter that we label ε with $0 < \varepsilon \ll 1$. It is for example the size of a phytoplankton colony divided by the depth of the water column. This extra information is essential to the analysis that is presented in this thesis. A system involving such a small parameter is called *perturbed*, and if this small parameter multiplies the highest partial derivative of an equation, we call this *singularly perturbed*. An example of a singularly perturbed reaction diffusion system is

$$\begin{aligned} u_t &= u_{xx} + f(u, v; \varepsilon), \\ v_t &= \varepsilon v_{xx} + g(u, v; \varepsilon). \end{aligned} \tag{1.2}$$

The models studied in this thesis are all singularly perturbed, and the mathematical tools that are used to analyze them exploit that perturbed character. After all, if ε is so small, why not simply set it equal to zero? In singularly perturbed problems, as is obvious in (1.2), simply equating $\varepsilon = 0$ drastically changes the character of the v-equation. It is not even a partial differential equation anymore. Therefore, the results that are derived using the limit problem for $\varepsilon = 0$ need to be studied with care. The mathematical field that is associated with these questions is usually referred to as *asymptotic analysis* or *perturbation analysis*. The results that are derived in this field have a validity regime that can be explicitly estimated in terms of the small parameter ε, as it asymptotically approaches zero.

In this section, we will provide an overview of several techniques from asymptotic analysis that are used throughout this thesis. They can be thought of as the prerequisites to the main part of this thesis, Chapters 2–5. The application of the techniques is not limited to reaction-diffusion systems, but concerns integrals or systems of ordinary differential equations with a small parameter ε. The partial differential equations treated in this thesis are in most cases converted

into systems of ordinary differential equations (for example by introducing a traveling wave coordinate), and after this reduction step, the techniques discussed in this chapter are applied. The techniques discussed in the prerequisites covered below, all define asymptotic results for ε approaching zero, and will in many cases be *leading order results* in ε. In order to quantify exactly what leading order means, we use the following definition.

Definition 1.0.1. Given two functions of a small parameter ε, $f(\varepsilon)$ and $\phi(\varepsilon)$, we say that

$$f(\varepsilon) = \mathcal{O}(\phi(\varepsilon)),$$

if there are constants k and $\bar{\varepsilon}$, both independent of ε, for which holds

$$|f(\varepsilon)| \leq k|\phi(\varepsilon)|, \quad \text{for} \quad 0 < \varepsilon < \bar{\varepsilon}.$$

We say that "f is big Oh of ϕ" or "f is of order ϕ" as ε approaches zero. In particular, a result holds 'to leading order in ε' if the error term is 'big Oh' of a positive power of ε, $\mathcal{O}(\varepsilon^p)$ with $p > 0$. Furthermore, we write $f \sim \phi$ as $\varepsilon \downarrow 0$ if

$$\lim_{\varepsilon \downarrow 0} \frac{f(\varepsilon)}{\phi(\varepsilon)} = 1.$$

These definitions are gained from [77].

1.1 Laplace's method

The first technique that we discuss is one that is not necessarily related to differential equations, but to an operation that is often used to solve them: integrals. Laplace's method is developed to approximate integrals of a product of two functions, say $f(t)h(t)$. Suppose that one of the factors of the product, $h(t)$, is localized; it has a well-defined maximum in the integration interval and the decay away from that maximum is 'fast'. Then, intuitively, one may expect that the product of $h(t)$ with $f(t)$, which may not be localized, can be approximated by using the value of $f(t)h(t)$ at the location in the integration interval where $h(t)$ is maximal. This is exactly what Laplace's method uses.

An example of a function with a particularly localized character is the exponential. Their growth rate is is fast, especially when the argument is very large. A function $h(t) = e^{\frac{g(t)}{\varepsilon}}$, with $g(t)$ some continuous, real-valued function, is thus strongly localized because the exponent grows asymptotically large as ε approaches zero. Laplace's approximation concerns therefore integrals of the form

$$\int_a^b f(t) e^{\frac{g(t)}{\varepsilon}} dt,$$

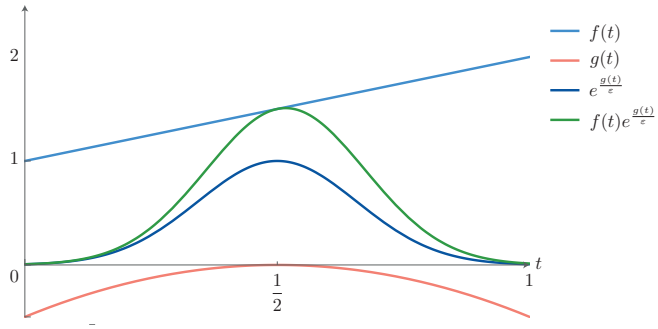

Figure 1.1: Illustration of localized function to which Laplace's method can be applied. Here, $f(t) = t + 1$ and $g(t) = -2(t - \frac{1}{2})^2$ and $\varepsilon = 0.1$.

where $f(t)$ and $g(t)$ are continuous functions over the bounded interval $[a, b]$ with $a < b$. For an illustration of this intuition, see Figure 1.1. We follow the notation from [77]. Laplace's method states that if the maximum of $g(t)$ in the interval $[a, b]$ is attained at some $t_0 \in (a, b)$ and $f(t_0) \neq 0$, then it holds that

$$\int_a^b f(t)e^{\frac{g(t)}{\varepsilon}}\,dt \sim f(t_0)\sqrt{\frac{2\pi\varepsilon}{g''(t_0)}}e^{\frac{g(t_0)}{\varepsilon}},$$

as $\varepsilon \to 0$. Note that the maximum value of f does not determine for the approximation but the second derivative of g does. It carries information on the steepness of the decay of g outside t_0; it says something about how localized the exponential function really is. This way, Laplace's method provides a direct asymptotic approximation for integrals in terms of local information that can easily be determined.

Say that $f(t) = t + 1$ and $g(t) = -2(t - \frac{1}{2})^2$. Then the maximum of $g(t)$ is attained at $t_0 = \frac{1}{2}$, and the integral $\int_0^1 f(t)e^{\frac{g(t)}{\varepsilon}}$ is approximated by $\frac{3\sqrt{\pi}}{2\sqrt{2}}\sqrt{\varepsilon}$, as $\varepsilon \to 0$. For $\varepsilon = 0.1$, the error that is made using Laplace's method is $-9.3 \cdot 10^{-4}$, which drops to $6.9 \cdot 10^{-18}$ for $\varepsilon = 0.001$.

It may be the case that the maximum of $g(t)$ is on one of the boundaries of the integration interval. In this case, too, Laplace's method provides estimates. For example, when the maximum of g is attained at the right boundary and , $t_0 = b$, and $g'(b) \neq 0$, we approximate

$$\int_a^b f(t)e^{\frac{g(t)}{\varepsilon}}\,dt \sim -\varepsilon\frac{f(b)}{g'(b)}e^{\frac{g(b)}{\varepsilon}}.$$

An analogous result exists for a maximum at the left boundary, $t_0 = a$, with a change of sign. Moreover, this result can be extended using higher order estimates if $g'(b) = 0$. Full proofs and higher order terms of this approximation can be found in, for example, [174].

1.2 Center manifold reduction

Upon studying systems of ordinary differential equations, one of the first techniques we learn is how to study the linear stability of fixed points in autonomous systems. That is, in a system of the form

$$\dot{x} = f(x),$$

with $\dot{x} = \frac{dx}{dt}$ and where $x \in \mathbb{R}^n$ and $f(x) : \mathbb{R}^n \to \mathbb{R}^n$ smooth enough. We learn that the linear stability of a fixed point x^* can be determined by linearizing the function f, that is, studying the Jacobian, $J(x)$. The behavior of the resulting Jacobian evaluated at the fixed point returns the stability of the fixed point. If all eigenvalues of $J(x^*)$ have negative real part, i.e. there are only *stable eigenvalues*, the fixed point is stable. If there is an eigenvalue with positive real part, i.e. an *unstable eigenvalue*, the fixed point is unstable. If, however, any of the eigenvalues has zero real part, a *center eigenvalue*, and there are no unstable eigenvalues, the linear stability analysis is inconclusive. The only way to determine the stability in that case is to do nonlinear stability analysis, and study the behavior of the system using the *center manifold theorem*, Theorem 1.2.2. A detailed proof of this theorem is given in [18], but we will explain the results here.

Suppose we are given a system of which the Jacobian at a fixed point only has n_s stable and n_c center eigenvalues and no unstable eigenvalues. Without loss of generality, we can then translate and rewrite the system in a normal form with a slight abuse of notation like

$$\begin{aligned} \dot{x} &= Ax + f(x, y), \\ \dot{y} &= By + g(x, y), \end{aligned} \tag{1.3}$$

where $x \in \mathbb{R}^{n_c}$ and $y \in \mathbb{R}^{n_s}$. A and B are constant coefficient, square matrices with dimensions n_c and n_s, respectively and the eigenvalues of A all have zero real part, while the eigenvalues of B only have negative real part. Moreover, the functions f and g are strictly nonlinear and smooth. In this normal form, the fixed point is translated to $(x, y) = (0, 0)$ and we have changed the coordinates so that the center and stable behavior are clearly separated. Then, the center manifold theorem states the following.

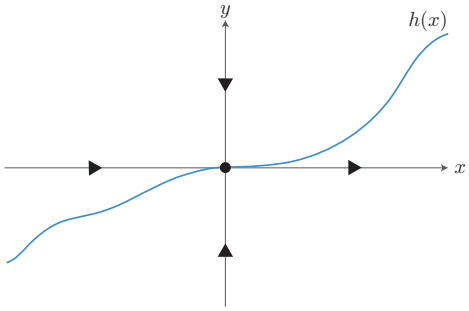

Figure 1.2: Illustration of a center manifold for system (1.3) in the case that $n_c = n_s = 1$. The stable subspace coincides with the y-axis and the center subspace with the x-axis.

Theorem 1.2.1 (Existence of a center manifold)**.** *The system* (1.3) *has a locally defined, invariant manifold*

$$W^c = \{(x, h(x)) : x \in \mathbb{R}^{n_c}, |x| < \varepsilon\},$$

where $\varepsilon > 0$ *is small enough and* $h(x) : \mathbb{R}^{n_c} \to \mathbb{R}^{n_s}$ *satisfies*

$$h(0) = 0, \qquad h_x(0) = 0.$$

That is, there exists a manifold on which the behavior of (1.3) is locally invariant (an initial point on the manifold that follows the flow induced by (1.3), stays on the manifold for some time). This manifold has the dimension of the number of center eigenvalues and is locally a graph over x. Moreover, the center manifold is tangent to the center eigenspace of the fixed point. An illustration of this idea with $n_c = n_s = 1$ is depicted in Figure 1.2

Additional to the existence of such a locally invariant manifold, there exists a theorem that states that the stability of the fixed point $(0, 0)$ of (1.3) can be determined by studying the behavior on that center manifold.

Theorem 1.2.2 (Center manifold reduction theorem)**.** *Locally near* $(0, 0)$*, the system* (1.3) *is topologically conjugate to the system*

$$\begin{aligned} \dot{x} &= Ax + f(x, h(x)), \\ \dot{y} &= By. \end{aligned} \tag{1.4}$$

Note that system (1.4) decouples, and for the stability of fixed point $(0, 0)$ it suffices to study the n_c-dimensional system defined by $\dot{x} = Ax + f(x, h(x))$.

That is a reduction of n_s dimensions as opposed to the system (1.3)! Theorem 1.2.2 is a local result, which means that it is only valid if the behavior of matrix B is significantly faster than that of A. That is, the eigenvalues of B must be significantly larger than $\mathcal{O}(\varepsilon)$; there is a spectral gap between the center and stable eigenvalues.

In a more general case, the system depends on parameters and only exhibits center eigenvalues for certain parameter combinations. For those combinations, the system changes stability; there is a bifurcation. Also in the case of a bifurcation, center manifold reduction can be of help, via the following theorem.

Theorem 1.2.3 (Center manifold reduction with parameter dependence)**.** *Consider the system*

$$\begin{aligned} \dot{x} &= A(\mu)x + f(x, y; \mu), \\ \dot{y} &= B(\mu)y + g(x, y; \mu), \end{aligned} \tag{1.5}$$

with $x \in \mathbb{R}^{n_c}$ and $y \in \mathbb{R}^{n_s}$ and $\mu \in \mathbb{R}^k$ a parameter. Let $A(0)$ be a constant coefficient matrix of dimension n_c with only center eigenvalues, and $B(0)$ a constant coefficient matrix of dimension n_s with only stable eigenvalues. Furthermore, let f and g be strictly nonlinear and smooth. Then, there exists a $\mathbb{R}^k$-dimensional family of locally invariant (i.e. for μ small enough) center manifolds

$$W^c_\mu = \{(x, h(x; \mu)) : x \in \mathbb{R}^{n_c}, |x| < \varepsilon\},$$

and $h(x; 0) = h(x)$ from Theorem 1.2.1. Furthermore, system (1.5) *is topologically conjugate with*

$$\begin{aligned} \dot{x} &= A(\mu)x + f(x, h_\mu(x); \mu), \\ \dot{y} &= B(\mu)y. \end{aligned} \tag{1.6}$$

This extension can be verified by adding to system (1.5) a auxiliary equation $\dot{\mu} = 0$, and applying Theorems 1.2.1 and 1.2.2. Again, this result is a local one; the reduction only holds for those μ that make the real part of the eigenvalues of B still significantly smaller than those of A. The perturbation by μ may not violate the spectral gap condition. Center manifolds can be determined explicitly, for more details on how to approach this, see for example [98].

1.3 WKB-method

The next perturbation method in this section of mathematical tools is one that approximates solutions to second order, non-autonomous, linear, ordinary

differential equations that are singularly perturbed. That is, differential equations of the form

$$\varepsilon^2 y_{xx} - q(x)y = 0, \tag{1.7}$$

with $x \in \mathbb{R}$ with $q(x) > 0$. To gain some intuition, first consider the case that $q(x) = q_0 > 0$, a constant. In that case, equation (1.7) is simply a second order differential equation with constant coefficients. It is solved by exponentials; the general solution is

$$y(x) = c_+ e^{\frac{\sqrt{q_0}}{\varepsilon}x} + c_- e^{-\frac{\sqrt{q_0}}{\varepsilon}x}, \tag{1.8}$$

where $c_\pm$ are two constants that depend on the initial conditions. The WKB-method[1] generalizes this idea of using exponentials for a q that depends explicitly on x. Because of the singularly perturbed nature of (1.7), it is expected that there is a separation of scales inherent to the equation. The specific assumption of the WKB-method is that the fastest[2] behavior is captured by an exponential function as a factor of the solution. Specifically, we assume that the solution is of the form

$$y(x) = e^{\frac{\theta(x)}{\varepsilon}} \left[y_0(x) + \varepsilon y_1(x) + \mathcal{O}(\varepsilon^2) \right], \tag{1.9}$$

where $\theta(x)$ and $y_i(x)$ are functions that need to be determined. Upon substituting (1.9) in to (1.7) and collecting terms of the same order in ε, we can rewrite to leading order

$$\varepsilon^2 \left\{ \frac{1}{\varepsilon^2}(\theta')^2 y_0 + \frac{1}{\varepsilon}\left[\theta'' y_0 + 2\theta' y_0' + (\theta')^2 y_1\right] \right\} - q(x)\left(y_0 + \varepsilon y_1\right) = 0, \tag{1.10}$$

where $'$ is the derivative with respect to x. The leading order terms of (1.10) make up the $\mathcal{O}(1)$ equation,

$$(\theta')^2 = q(x), \tag{1.11}$$

which yields $\theta(x) = \pm \int^x \sqrt{q(s)} ds$. The next order equation of (1.10) is

$$\theta'' y_0 + 2\theta' y_0' + (\theta')^2 y_1 = q(x) y_1, \tag{1.12}$$

but using (1.11), this simplifies to $\theta'' y_0 + 2\theta' y_0' = 0$, which has solution

$$y_0(x) = \frac{c}{\sqrt{\theta'}},$$

[1] WKB stands for Wentzel, Kramers, and Brillouin who worked in the field of quantum mechanics, and used this method to find approximate solutions to the Schrödinger equation. There are, however, several other names for the same technique.

[2] Here, fast indicates a big change in y over a short x-interval.

where c is an integration constant. Now recall that there are two solutions for $\theta(x)$. This is to be expected in a second order equation without initial conditions; compare with the solution (1.8) which is also a linear combination of two exponentials. Combining the results of the two orders of magnitude in this method and making a linear combination of the two solutions for θ, we find a leading order approximation to (1.7),

$$y(x) = \frac{1}{q^{\frac{1}{4}}(x)} \left[C_+ e^{\frac{1}{\varepsilon}\int^x \sqrt{q(s)}ds} + C_- e^{-\frac{1}{\varepsilon}\int^x \sqrt{q(s)}ds} \right]. \tag{1.13}$$

To find higher order terms of this approximation, we can return to equation (1.10) and collect the next order's terms to solve y_1 and continue. Note that the solution for $y(x)$ is not well-defined for values of x at which $q(x)$ vanishes. In this case, we speak of *turning points*, extra measures are needed and the solution at those x-values is usually approximated using Airy functions. For more details, see [77].

1.4 Geometric singular perturbation theory

In singular perturbed systems, often a separation in (time) scales can be observed. For example, localized behavior of solutions, very steep transitions near boundaries, or oscillations with a fast and a slow part. Taking this type of information into account improves the prospects of solving the system tremendously. By considering both scales of a perturbed problem separately, we can usually derive results much more easily. Moreover, the concatenation of the fast and slow scale is shown to be a good (local) approximation of the original problem. The question that remains is then how the two worlds meet. For at least a class of singularly perturbed problems, geometric singular perturbation theory (GSPT) provides the answer to just that. In this section the main results of the theory are formulated and interpreted. We follow mainly the formulations from [73] and [149], and conclude this subsection with an example where the results are applied to the forced Van der Pol equations.

The focus to which we apply GSPT is a class of systems of ordinary differential equations of the following form,

$$\begin{aligned} \dot{u} &= f(u, v, \varepsilon), \\ \dot{v} &= \varepsilon g(u, v, \varepsilon), \end{aligned} \tag{1.14}$$

where $\dot{} = \frac{d}{dt}$, $u \in \mathbb{R}^k$ and $v \in \mathbb{R}^l$ with $k, l \geq 1$. For the functions f and g we will require them to be 'smooth enough' for the application of the theorems. Furthermore, $0 < \varepsilon \ll 1$ is, of course, a small parameter and f, g are $\mathcal{O}(1)$ with respect to ε.

Upon introducing a new time scale, $\tau = \varepsilon t$, we can rewrite system (1.14) into an equivalent formulation thereof;

$$\begin{aligned} \varepsilon u' &= f(u, v, \varepsilon), \\ v' &= g(u, v, \varepsilon), \end{aligned} \tag{1.15}$$

where $' = \frac{d}{d\tau}$. Since ε is small, τ is a much slower time scale compared to t. Hence, we refer to (1.15) as the slow system, opposing the label 'fast' for system (1.14). This is the setting to which GSPT applies.

1.4.1 Fenichel's theorems

The two equivalent systems (1.14) and (1.15) describe the same behavior, but in a different variable. One could say that the two systems argue from a different viewpoint. Taking the limit $\varepsilon \to 0$ in (1.14) yields the so-called *layer system*,

$$\begin{aligned} \dot{u} &= f(u, v, 0), \\ \dot{v} &= 0, \end{aligned} \tag{1.16}$$

and is not at all equivalent to the limiting system of (1.15), which we call the *reduced system*,

$$\begin{aligned} 0 &= f(u, v, 0), \\ v' &= g(u, v, 0). \end{aligned} \tag{1.17}$$

The layer system has trivial behavior in the v-components, making it significantly easier to study, and the reduced system is a differential-algebriac system, where the dynamics is restricted to the manifold on which $f(u, v, 0) = 0$. This generically l-dimensional manifold, the *critical manifold*,

$$\mathcal{M} = \{(u, v) \in \mathbb{R}^{k+l} : f(u, v, 0) = 0\}, \tag{1.18}$$

is, in turn, exactly the set of fixed points of the layer system. Hence, in terms of the layer problem the only nontrivial behavior is in the u-direction, and its direction generically reverts at $\mathcal{M}$. On the other hand, the reduced problem only takes place on the critical manifold, and the dynamic behavior is dictated by the v-equation. And since (1.16) is associated with the fast, and (1.17) with the slow coordinate, we can conclude that the fast behavior is to leading order trivial in the v-direction and determined by u, while the leading order slow behavior takes place in the lower dimensional state space defined by $\mathcal{M}$ and determined by v.

Definition 1.4.1. Let $\mathcal{M}_0 \subset \mathcal{M}$ be a compact subset of the critical manifold corresponding to system (1.17). If the eigenvalues of the Jacobian $\frac{\partial f}{\partial u}(u, v, 0)|_{\mathcal{M}_0}$ are bounded away from the imaginary axis, then the critical manifold is *normally hyperbolic*.

The evident question to ask now is how to make the results drawn from both limiting systems compatible. This is established by Fenichel's theory [49], and will be explained according to two theorems and one corollary.

Theorem 1.4.1 (Fenichel's first theorem)**.** *Suppose $\mathcal{M}_0$ is compact and normally hyperbolic. Then, for $\varepsilon > 0$ and sufficiently small there exists a manifold $\mathcal{M}_\varepsilon$ which is $\mathcal{O}(\varepsilon)$ close to $\mathcal{M}_0$ and diffeomorphic to it. Moreover, $\mathcal{M}_\varepsilon$ is locally invariant under the flow of* (1.14)*.*

Like the center manifold in section 1.2, the persisting manifold $\mathcal{M}_\varepsilon$ is locally a graph over the v-coordinates, say $u = h(v)$; this follows from the Implicit Function Theorem and the fact that $\mathcal{M}_0$ is normally hyperbolic. Hence, we can reduce the reduced system to

$$v' = g(h(u), v, 0).$$

So, even for $\varepsilon \neq 0$ but small enough, the slow flow may be approximated by (1.17). The slow flow takes place on the locally invariant *slow manifold* $\mathcal{M}_\varepsilon$. For precise statements on the smoothness and invariance of $\mathcal{M}_\varepsilon$, see [82, 84].

It is noteworthy what happens when a critical manifold is not normally hyperbolic. Say, for instance, that $\mathcal{M}$ is folded so the Jacobian has a zero eigenvalue. In most cases, these folds are sets of *jump points*. At those points, the flow starts to follow the fast vector field because that is then the dominant term. However, one needs to be very careful with this assumption because if there is a critical point of the slow flow near the fold, completely different mechanisms can occur. This is further detailed in section 1.4.2 .

The interplay between the slow behavior and the fast phase space that surrounds it, is defined by the stable and unstable manifolds of the points on the critical manifold. Say these sets are $W^{s,u}(\mathcal{M}_0)$, then Fenichel's second theorem specifies their persistence if $\varepsilon \neq 0$.

Theorem 1.4.2 (Fenichel's second theorem)**.** *Suppose $\mathcal{M}_0 \subset \mathcal{M}$ is compact and normally hyperbolic. Then for $\varepsilon > 0$ and sufficiently small, there exist manifolds $W^s(\mathcal{M}_\varepsilon)$ and $W^u(\mathcal{M}_\varepsilon)$ that are $\mathcal{O}(\varepsilon)$ close and diffeomorphic to $W^s(\mathcal{M}_0)$ and $W^u(\mathcal{M}_0)$, respectively. Moreover, these manifolds are locally invariant under the flow of* (1.14)*.*

The stable and unstable manifolds of $\mathcal{M}_\varepsilon$ decay to $\mathcal{M}_\varepsilon$ with an exponential rate. Often, bounded solutions to (1.14) start in a neighborhood of slow manifold $\mathcal{M}_\varepsilon$, follow $W^u(\mathcal{M}_\varepsilon)$ away from $\mathcal{M}_\varepsilon$ and return to it via $W^s(\mathcal{M}_\varepsilon)$. Hence, the intersection $W^s(\mathcal{M}_\varepsilon) \cap W^u(\mathcal{M}_\varepsilon)$ is in many cases a focus of study.

Fenichel's first and second theorem already allow us to draw significant conclusions. If, for example, $\mathcal{M}_0$ is purely attracting, studying the slow behavior

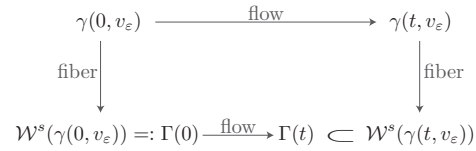

Figure 1.3: Diagram corresponding to Fenichel's third theorem. For $v_\varepsilon \in \mathcal{M}_\varepsilon$, the set that results from flowing forward its fiber is a subset of the fiber of the forward flown initial point v_ε.

on $\mathcal{M}_\varepsilon$ may be enough, because all initial points will eventually be attracted to $\mathcal{M}_\varepsilon$. The simple concatenation of pieces of fast and slow orbit for $\varepsilon = 0$ makes up what we label a *singular orbit*. We say that a singular orbit persists for $\varepsilon \neq 0$, if the construction of it is valid for any ε with $0 < \varepsilon < \varepsilon_0$. The proofs of persistence of orbits often rely on the transverse intersections of manifolds, of which we know they persist.

Fenichel's second theorem guarantees persistence of the stable and unstable manifolds of $\mathcal{M}_0$ as an analogous object. However, this does not imply the persistence of the stable and unstable manifold of a specific point on $\mathcal{M}_0$. After all, a critical point v_0 on $\mathcal{M}_0$ does in general not even perturb to a fixed point for $\varepsilon \neq 0$. Still, Fenichel's third theorem explains that indeed $W^{s,u}(v_0)$ perturb to something analogous in an $\mathcal{O}(\varepsilon)$ neighborhood. As the exact statement of this theorem requires quite some notation, we explain the correspondence using Figure 1.3 and a corollary of the theorem.

Let v_ε be a point in $\mathcal{M}_\varepsilon$, then, by Fenichel's first theorem, there exists a $v_0 \in \mathcal{M}_0$ that can be associated with it in a natural way, and v_0, being a fixed point of the layer system (1.16), has stable and unstable manifolds $W^{s,u}(v_0)$. Then, Fenichel's third theorem states that there exist manifolds $\mathcal{W}^{s,u}(v_\varepsilon)$ which are diffeomorphic and $\mathcal{O}(\varepsilon)$ close to $W^{s,u}(v_0)$, which we call *fibers* of v_ε. The fibers $\mathcal{W}^{s,u}(v_\varepsilon)$ are not stable and unstable manifolds (since v_ε is not a fixed point) nor are they invariant. There is, however, a weaker sense of invariance available for the fibers, which is explained by Figure 1.3.

Denote any orbit of system (1.14) parametrized by t and with initial point $v_\varepsilon \in \mathcal{M}_\varepsilon$ as $\gamma(t; v_\varepsilon)$. Then, let the corresponding fiber $\mathcal{W}^s(v_\varepsilon)$ be the stable fiber of v_ε. This fiber is in itself a set of initial conditions, say $\Gamma(0)$, where

$$\Gamma(t) = \{\gamma(t, x) : x \in \mathcal{W}^s(v_\varepsilon)\}.$$

Fenichel's theorem states that the set $\Gamma(t)$ is a subset of the fiber of $\gamma(t, v_\varepsilon)$, $\mathcal{W}^s(\gamma(t, v_\varepsilon))$, see Figure 1.3.

From Fenichel's third theorem, the corollary below follows.

Corollary 1.4.3. *Suppose $\mathcal{M}_\varepsilon$ is a slow manifold as defined in Fenichel's first theorem. Let $\gamma(t, v_\varepsilon) \subset \mathcal{M}_\varepsilon$ be an orbit in the slow manifold with $\gamma(0, v_\varepsilon) = x$, $x \in \mathcal{M}_\varepsilon$. Then there exists a* base point *$v_\varepsilon^+ \in \mathcal{M}_\varepsilon$ and an orbit $\gamma^+(t, v_\varepsilon^+)$ with $\gamma^+(0, v_\varepsilon^+) = v_\varepsilon^+$ for which there exist constants $C_1, C_2, k > 0$ such that*

$$||\gamma(t, v_\varepsilon) - \gamma^+(t, v_\varepsilon^+)|| \leq C_1 e^{-k/\varepsilon} \quad \textit{for} \quad t \geq \frac{C_2}{\varepsilon}.$$

Hence, Fenichel's theorems prescribe the behavior of singularly perturbed systems like (1.14) to leading order. It provides insight in how slow and fast limiting behavior can be 'glued' together. If normal hyperbolicity of the manifold is lost, the theorems are unfortunately no longer applicable. In these cases, the behavior requires canard theory.

1.4.2 Canard theory

When a critical manifold is not normally hyperbolic, see Definition 1.4.1, the fast behavior generically takes over because this is the dominant mechanism. In special cases, however, an orbit remains close to the critical manifold for an $\mathcal{O}(1)$ time, even though it enters a repelling branch of the critical manifold. Such orbits are the focus of study in canard theory. For a clear presentation of this theory, we follow [149] and restrict to three dimensions in (1.14). In particular, we say $k = 1$ and $l = 2$ and study

$$\begin{aligned} \varepsilon u' &= f(u, v_1, v_2, \varepsilon), \\ v_1' &= g_1(u, v_1, v_2, \varepsilon), \\ v_2' &= g_2(u, v_1, v_2, \varepsilon), \end{aligned} \tag{1.19}$$

where $' = \frac{d}{d\tau}$. Canard theory applies to GSPT problems of at least dimension 3 in the case that the critical manifold loses normal hyperbolicity. To guarantee that this happens in (1.19) close to the origin in a non-degenerate way, we assume

$$\begin{aligned} f(0,0,0,0) &= 0, \qquad & f_u(0,0,0,0) &= 0, \\ f_{v_1}(0,0,0,0) &\neq 0, \qquad & f_{uu}(0,0,0,0) &\neq 0, \end{aligned} \tag{1.20}$$

which are simply conditions on the critical manifold $\mathcal{M}$ as defined in 1.4. Making use of the Implicit Function Theorem, we can now parametrize a fold-curve F by $(h_1(v_2), h_2(v_2), v_2) \in \mathbb{R}^3$. Furthermore, we define a transversality criterion,

$$\ell(v_2) := \left\langle \begin{pmatrix} f_{v_1} \\ f_{v_2} \end{pmatrix}, \begin{pmatrix} g_1 \\ g_2 \end{pmatrix} \right\rangle \Bigg|_{(h_1(v_2), h_2(v_2), v_2, 0)}, \tag{1.21}$$

following [149]. This transversality criterion determines the behavior of the reduced flow near the fold curve. In the case that $\ell(0) \neq 0$, the point on F is a

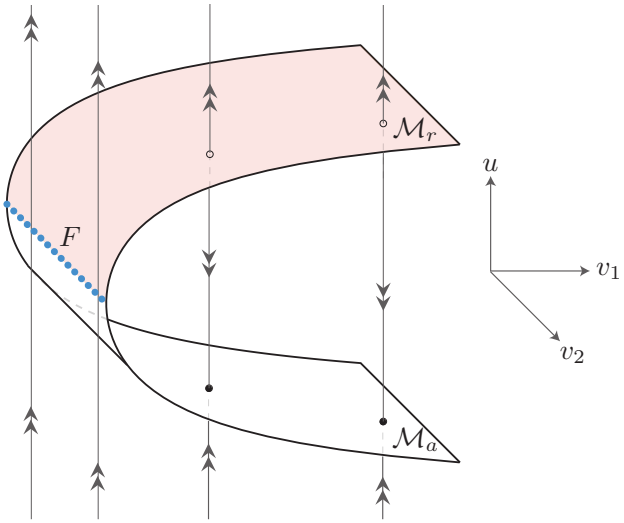

Figure 1.4: Schematic illustration of the folded critical manifold with repelling and attracting branches $\mathcal{M}_r$ and $\mathcal{M}_a$, and the fold curve F.

jump point, as was discussed in the previous paragraph. If, however $\ell(0) = 0$, it is not, and these points are called *canard points*.

In the case that $\ell(0) = 0$ and (1.20) are satisfied, the system can be transformed into a normal form by a smooth change of coordinates. This normal form is

$$\begin{aligned} \varepsilon u' &= u^2 + v_1 \quad &&+\mathcal{O}(\varepsilon v_1, \varepsilon v_2, \varepsilon u, \varepsilon^2, v_1^2 u, u^3, v_1 v_2 u), \\ v_1' &= au + bv_2 &&+\mathcal{O}(v_1, \varepsilon, v_2^2, v_2 u, u^2), \\ v_2' &= c &&+\mathcal{O}(v, \varepsilon, v_2, u), \end{aligned} \tag{1.22}$$

where $a, b, c \in \mathbb{R}$ are explicitly computable. This transformation simply translates F to the v_2-axis, and uses the fact that the critical manifold is locally parabolic. See a schematic representation in Figure 1.4. The error terms are quantified, but since we work locally around the origin, we will say that (1.22) is to leading order equal to

$$\begin{aligned} \varepsilon u' &= u^2 + v_1, \\ v_1' &= au + bv_2, \\ v_2' &= c, \end{aligned} \tag{1.23}$$

for a clear presentation. The critical manifold of (1.23) is

$$\mathcal{M} = \{u^2 + v_1 = 0\} = \{(u, v_1(u, v_2), v_2) \in \mathbb{R}^3\},$$

because it is a graph over (u, v_2) with $v_1(u, v_2) = -u^2$. Differentiating v_1 with respect to τ yields $v_1' = -2uu'$ and substituting this into (1.23) we reduce on $\mathcal{M}$ to

$$\begin{aligned} -2uu' &= au + bv_2, \\ v_2' &= c. \end{aligned} \tag{1.24}$$

Which defines the reduced flow on $\mathcal{M}$ in the (u, v_2) field, on which $u = 0$ coincides with the F. For $u = 0$, the system is singular; we desingularize it by reparametrizing the orbits via the substitution $\xi(\tau)$ with $\frac{d\xi}{d\tau} = \frac{1}{-2u}$, and obtain the *desingularized system*

$$\begin{aligned} u_\xi &= au + bv_2, \\ v_\xi &= -2cu. \end{aligned} \tag{1.25}$$

The phase portraits of (1.24) and (1.25) are equivalent, apart from the direction of the orbits. If $u > 0$, the direction of orbits in (1.25) needs to be reversed to represent those of (1.24), see Figure 1.5. Note that $(0, 0)$ is an equilibrium of (1.25), but not of (1.24). This defines $(0, 0)$ to be a *folded singularity* in (1.24). The character of the folded singularity is determined by the character of the equilibrium of (1.25). The eigenvalues of the Jacobian of (1.25) at $(0, 0)$ are $\lambda_{1,2} = \frac{1}{2}(a \pm \sqrt{a^2 - 8bc})$. For now, we assume that $bc < 0$, so $(0, 0)$ is a saddle. Consequently, the point $(0, 0)$ in (1.24) is a *folded saddle*. By scaling the saddle back in the τ variable, we find that $(0, 0)$ in fact admits two orbits passing through the fold curve, see Figure 1.5. The solutions of the reduced problem passing from the attracting to the repelling branch of the critical manifold are called *singular canards*, while solutions of the reduced problem that pass from the repelling part of the critical manifold to the attracting branch are *singular faux canards*.

Using blow-up techniques, which are not within the scope of this thesis, it can be shown that, in fact, near a folded saddle, the singular canard persists as a solution of the full system (1.22), see [149]. The theory for three dimensions can be generalized to n, see for example [166].

1.4.3 Example: The forced Van der Pol equations

In this section, we apply GSPT and Canard theory to the forced Van der Pol equation, to exemplify the potential of the theory. It was originally proposed in

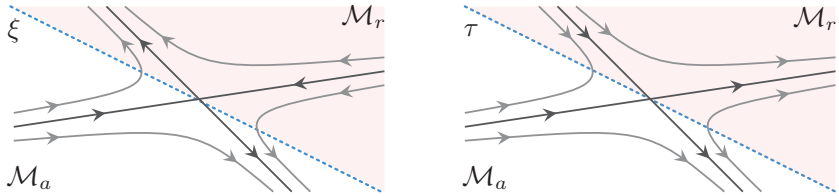

Figure 1.5: Left: Saddle fixed point of the desingularized system (1.25) parametrized by ξ. Right: The corresponding folded saddle of (1.24).

[158] and applies to electrical circuits employing vacuum tubes. Central to this paragraph are thus,

$$\begin{aligned} \dot{u} &= u - \frac{1}{3}u^3 + v_1, \\ \dot{v}_1 &= \varepsilon(-u + \sqrt{2}\cos(v_2)), \\ \dot{v}_2 &= \varepsilon \end{aligned} \tag{1.26}$$

where $\dot{} = \frac{d}{dt}$. The system is equivalently posed in the slow time scale $\tau = \varepsilon t$.

$$\begin{aligned} \varepsilon u' &= u - \frac{1}{3}u^3 + v_1, \\ v_1' &= -u + \sqrt{2}\cos(v_2), \\ v_2' &= 1. \end{aligned} \tag{1.27}$$

The limiting sytems are

$$\begin{aligned} \dot{u} &= u - \frac{1}{3}u^3 + v_1, & 0 &= u - \frac{1}{3}u^3 + v_1, \\ \dot{v}_1 &= 0, & v_1' &= -u + \sqrt{2}\cos(v_2), \\ \dot{v}_2 &= 0 & v_2' &= 1. \end{aligned} \tag{1.28}$$

The critical manifold is defined by $v_1 = \frac{1}{3}u^3 - u$ and has two fold curves at $u = \pm 1$ which are parametrized by v_2. The fast behavior is trivial in the v_1 and v_2 direction while $\dot{u}$ changes sign exactly at the critical manifold. This is depicted in the (u, v_1)-plane in Figure 1.6. On the critical manifold, the singular system that is obtained by differentiating $v_1 = \frac{1}{3}u^3 - u$ defines the slow flow,

$$\begin{aligned} (u^2 - 1)u' &= -u + \sqrt{2}\cos(v_2), \\ v_2' &= 1, \end{aligned} \tag{1.29}$$

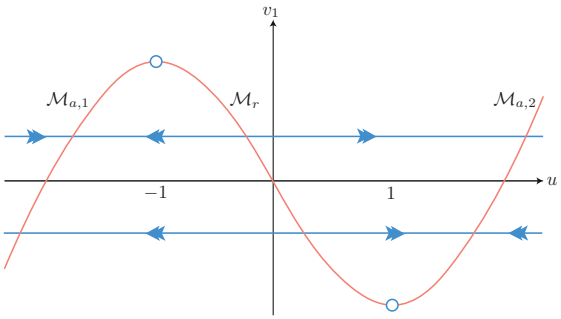

Figure 1.6: Slow manifold and fast singular flow of (1.26) in the (u, v_1) field, for a fixed v_2. The open circles are fold points of the critical manifold $\mathcal{M} = \mathcal{M}_{a,1} \cup \mathcal{M}_r \cup \mathcal{M}_{a,2}$.

which is desingularized by introducing $\xi(\tau)$ with $\frac{d\xi}{d\tau} = \frac{1}{u^2-1}$, to obtain,

$$\begin{aligned} u_\xi &= -u + \sqrt{2}\cos(v_2), \\ v_{2,\xi} &= u^2 - 1. \end{aligned} \tag{1.30}$$

The desingularized system has equilibria

$$(u, v_2) = \left(1, \pm\frac{\pi}{4} + 2k\pi\right), \qquad (u, v_2) = \left(-1, \pm\frac{3\pi}{4} + 2k\pi\right) \quad \text{for} \quad k \in \mathbb{Z}.$$

where $(1, -\frac{\pi}{4} + 2k\pi)$ and $(-1, \frac{3\pi}{4} + 2k\pi)$ are of saddle type, and $(1, \frac{\pi}{4} + 2k\pi)$ and $(-1, -\frac{3\pi}{4} + 2k\pi)$ are foci, see the phase portrait in Figure 1.7.

Changing the direction of the flow for $u < -1$ and $u > 1$ yields the phase portrait of (1.29), where the foci and saddle equilibria turn into folded singularities. Using Fenichel's theorems, we know that $\mathcal{M}$, as well as its stable and unstable manifolds persist for $\varepsilon \neq 0$, away from the fold lines. Note that if the canard point is a saddle, canard theory implies that a canard solution persists. Hence, there is a canard solution that, for example, $v_2 = -\frac{\pi}{4}$ passes through the canard point from the attracting to the repelling manifold. It then follows the repelling manifold closely for an $\mathcal{O}(1)$ amount of time, before the fast field takes over and sends it to the attracting manifold again. Because v_2 does not change to leading order in the fast behavior, it can even be shown that such a canard solution can be periodic. Projected onto the (u, v_1)-plane, such a solution is depicted in Figure 1.8.

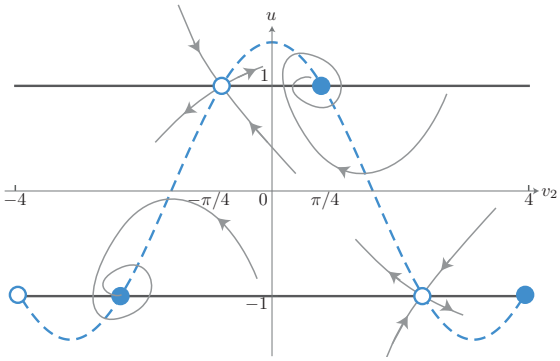

Figure 1.7: Phase portrait of (1.30). The blue closed circles denote foci, while open circles are saddle equilibria. The dashed curve is a nullcline for u, and the horizontals at $u = \pm 1$ are nullclines for v_2.

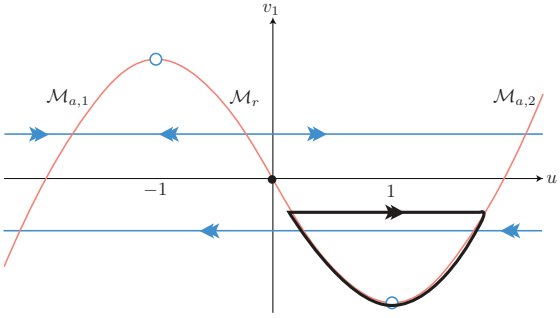

Figure 1.8: Example of a canard solution of (1.26) projected onto the (u, v_1)-plane, which passes through the canard point $(u, v_1, v_2) = (1, -\frac{2}{3}, -\frac{\pi}{4})$.

1.5 Outline of this thesis

This thesis shows an omnibus of studies of singularly perturbed reaction-diffusion systems with applications in various fields. Each system that is studied, requires a different approach using appropriate mathematical tools. Primarily, this is because the corresponding application describes a different type of solution (stationary pulse, traveling front, traveling pulse). Another reason is of a more practical nature; since the singularly perturbed character does not present itself in the same way, not every perturbation technique can be applied effectively. Roughly speaking, the models studied in this thesis have been motivated by three natural phenomena, which we discuss successively.

1.5.1 Blooming phytoplankton

The natural phenomenon that is studied in Chapters 2 and 3 is the blooming of phytoplankton. Among the plankton species, phytoplankton can be distinguished by the feature that it performs photosynthesis; it is a plant in the ocean. It forms the basis of the aquatic food chain and transports enormous amounts of carbon dioxide into the deep ocean and produces oxygen in return. Hence, phytoplankton populations may play a crucial role in understanding climate change, see [47]. Furthermore, field observations describe that phytoplankton colonies always choose a specifically preferred depth in the vertical water column. The two processes that specify this depth are the availability of light and nutrient. If there is an abundance of nutrients, the preferred depth is at the surface of the water column, because it optimizes light, this pattern is called a *surface scum*. If the water column is not very deep and light reaches all the way to the bottom, the phytoplankton prefers to sit at the bottom because of the best availability of nutrients, this state is a *benthic layer*. However, if the water column is very deep and nutrients are limited as well, phytoplankton optimizes its location somewhere in between and we label this a *deep chlorophyll maximum*, [79, 89]. This localized structure, as well as the observation in [78] that deep chlorophyll maxima often oscillate and may even exhibit chaotic behavior, were the inspiration for mathematicians to work on the subject.

Central to Chapters 2 and 3 is a model that consists of two differential equations for the concentration of phytoplankton and its nutrients, respectively. Before the establishment of those chapters, the mathematical framework was laid out in [176] and [177]. In [177], the linear stability of the so-called background state, where there is no phytoplankton and a constant nutrient concentration is studied. The spectrum of the linearized differential operator separates into two sets: one with eigenvalues λ_i (ordered so that $\lambda_i \leq \lambda_{i+1}$) which are $\mathcal{O}(\varepsilon^{1/3})$ apart and depend on parameters, and one with eigenvalues μ_i which are $\mathcal{O}(\varepsilon)$

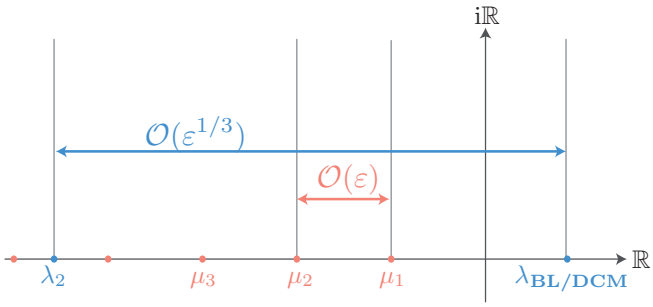

Figure 1.9: Schematic illustration of the spectrum of the background state of the phytoplankton model discussed in Chapters 2 and 3. Depending on parameters, the largest eigenvalue may change type.

interspaced, do not depend on parameters and are always negative. Furthermore, depending on the sinking velocity of the phytoplankton, the largest eigenvalue λ_1 may be either λ_{BL} or λ_{DCM}. That is, depending on that parameter, the primary bifurcation that the backgrounds state can undergo implies either the formation of a benthic layer, or that of a deep chlorophyll maximum, see Figure 1.9 for a illustration. This result is established by approximating the eigenfunctions corresponding to these eigenvalues using the WKB-method, see Section 1.3.

The bifurcation analysis in [177] provides analytic results for the primary (transcritical) bifurcations of the background state. Numerical analysis reported in the same article shows that, in the parameter regime where a DCM bifurcates, there is a secondary bifurcation of Hopf type. That implies that after the emergence of a DCM profile, it starts to oscillate in time. The two bifurcations occur in a $\mathcal{O}(\varepsilon)$ regime in parameter space, see Figure 1.10.

The Hopf bifurcation of the DCMs is studied analytically in [176]. By Fourier decomposing the linear stability problem of the background state into eigenfunctions, the primary, transcritical bifurcation is recovered using center manifold reduction, see Section 1.2. In principle, the local invariance of the center manifold is no longer guaranteed when λ_{DCM} is commensurate with the other eigenvalues μ_i. However, using a novel asymptotic approach and by studying the amplitude equations of the bifurcating profile, the center manifold reduction is extended beyond the spectral gap regime. Then, for $\lambda_{\mathrm{DCM}} = \mathcal{O}(\varepsilon)$, the Hopf bifurcation of the DCM profile is found analytically using, among other tools, Laplace's method, see Section 1.1.

In Chapter 2, this method of extending the validity of center manifold reduction is unfolded. We do this using a dummy model that is in some sense

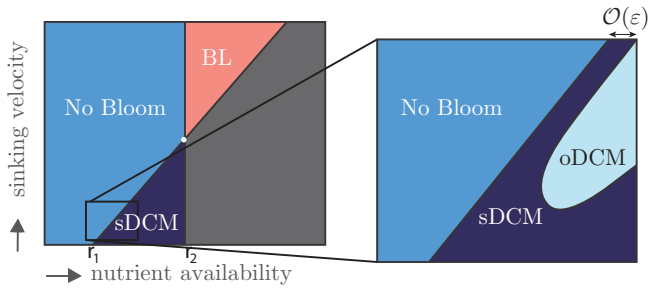

Figure 1.10: Schematic illustration of the bifurcations of the background state of the phytoplankton model discussed in Chapters 2 and 3, depending on the parameters that model nutrient availability and sinking velocity of the phytoplankton. The full model is discussed in Chapters 2 and 3. In the regime 'No Bloom', the background state is stable, the BL regime indicates the emergence of a benthic layer, and sDCM the emergence of stationary deep chlorophyll maxima. Lastly, oDCM is the regime where the DCM has undergone a Hopf bifurcation and oscillates consequently.

more general than the phytoplankton model because the reaction terms are general functions. On the other hand it is also simpler because particular intricacies of the phytoplankton model were not taken into account in order to declutter the presentation of the method. In that chapter we also aptly term this novel method *extended center manifold reduction* (ECMR). Indeed, in the dummy model we recover the classical center manifold reduction that indicates a transcritical bifurcation, as well as requirements for a secondary Hopf bifurcation. Furthermore, to exemplify the strength of ECMR, we apply the method to several other models and study the fate of codimension 2 bifurcations and even find low-dimensional chaos that is described by the extended center manifold reduction. The potential of ECMR is further substantiated by the fact that the low-dimensional chaos in the extended reduction persists in the full PDE model. Chapter 2 was published in full *Physica D* in 2015, see [139].

In Chapter 3 we return to the phytoplankton model and apply ECMR to the regime where a benthic layer emerges from the background state. The clean unfolding of the mechanism in Chapter 2 makes the application of it much more transparent compared to the pioneering article [176]. Chapter 3 reproduces briefly the result that a DCM can undergo a Hopf bifurcation, but also shows in more detail that, conversely, a benthic layer remains stable in the validity regime of ECMR. Because the phytoplankton model is quite detailed, the asymptotic analysis is challenging. Here too, the WKB and Laplace's method are applied.

Chapter 3 was published in full *Chaos* in 2015, see [41].

1.5.2 Spreading of malignant tumor

In ecology, a phenomenon called the *Allee effect* describes a threshold in the growth of a population. The causes of such an effect are numerous. For example, in small populations the gene pool may not be large enough for effective reproduction or finding a mate may be nearly impossible. This Allee effect has been observed in many applications, and recently, evidence has been gathered that in tumor growth this effect plays a role too. Intuitively, this can be motivated by the mere fact that small tumors are expected to be less threatening, but a more extensive literature overview related to the Allee effect in tumor spread can be found in the introduction of Chapter 4.

In modeling tumor spread, we focus on how it invades into its healthy surroundings. In the viewpoint of Chapter 4 it does so via hapto- or chemotaxis through the extracellular matrix. That is, the movement of the tumor is in the direction of the gradient of its healthy surrounding. As a simplified representation of the situation, we assume that the focus on a one-dimensional spatial domain is sufficient. This could be attained, for example, for tumors in two-dimension with a certain geometric symmetry that reduces the dimension. Mathematically, an invading tumor corresponds to a traveling front; a fixed spatial profile on an infinitely long, one-dimensional domain with different boundary conditions on both sides, moving with a constant speed. Since the type of tumors considered in Chapter 4, such as melanoma, have a very sharp edge [108], the transition from the left to the right boundary condition should be steep.

Although there are many ways to model the mechanism responsible for the growth of tumors, we study the consequences of incorporating the Allee effect in a model that was proposed in [125] and later adjusted and analysed in [67]. The former is a reaction-advection system and the latter also incorporates diffusion in the two components corresponding to tumor cell density and extracellular matrix. Both models assume that the growth of tumor cells is logistic; the growth term is quadratic so that the growth rate increases until the population gets close to the carrying capacity of the system. After that, the growth rate decreases but the growth term is still positive. For w being tumor cells, this logistic growth term can be presented by $f(w) = w(1 - w)$, if the carrying capacity is scaled to 1. A growth threshold following from the Allee effect is modeled in the system by substituting the quadratic term by a cubic one, $f(w) = w(1 - w)(w - \alpha)$, where α is the strength of the Allee effect.

In [67], the reaction-diffusion-advection tumor model is shown to exhibit four types of traveling wave solutions of which three exhibit a shock. This shock is a very steep transition – the edge of a tumor – and is explained by a canard

solution that is repelled from the repelling branch of a folded slow manifold and touched back upon the attracting branch of that manifold. One of these types of solutions has semi-compact support; on one side of the shock the tumor density is equal to zero, not only exponentially decaying to it. This type of solution is considered the most realistic because it models a sharply defined edge of a tumor. However, three out of four types of traveling wave solutions are deemed stable in [67] because they were observed numerically.

The effect of using an Allee threshold in the tumor growth term is two-fold. Following the methods used in [67], we first prove that only the shock solution with semi-compact support can exist, making the Allee model studied in Chapter 4 already preferable over the logistic growth model. Second, another agreement with experimental observations is found. This observation relates the invasion speed of a tumor to the collagen (the dominant ingredient in the extracellular matrix) density, i.e. the background state of the extracellular matrix. The results show that this relationship is *biphasic*, i.e. not monotonic but with a well-defined maximum. This biphasic relationship is also supported by the Allee model, while not being a feature of the logistic growth model.

The mathematical analysis in Chapter 4 relies heavily on geometric singular perturbation theory and canard theory, as briefly explained in Section 1.4. Chapter 4 was published in full in *Journal of Theoretical Biology* in 2016, see [140].

1.5.3 Traveling vegetation stripes

The last natural phenomenon to which reaction-diffusion models are applied in this thesis sets place in semi-arid regions of the earth. In times that the desert is expanding and this phenomenon is addressed as one of by-products of climate change, these half-barren transition regions are important focus points. Indeed, examples of these types of studies are abundant in literature, not in the least place in the applied mathematical journals.

The transition of vegetated areas into bare soil, *desertification*, occurs in several stages in which the vegetation displays itself in strikingly regular patterns of labyrinth, spotted, or striped character [106]. In the absence of grazing and on gentle slopes, it is mostly striped patterns which are observed, and due to the surplus of water uphill, they slowly migrate upwards. This subphenomenon of desertification is the focal point of Chapter 5.

The model that we use to analyze these patterns is of reaction-diffusion-advection type and models the interaction of water and vegetation density on sloped terrains. It resembles two predecessors; the Klausmeier model [88] and the Gray-Scott model [62], but incorporates the dominant pattern forming mechanisms of both. Our model is defined on a two-dimensional surface – the soil,

but since stripes are trivial in one direction, proving the existence of such solutions is essentially one-dimensional. The type of solution that corresponds to stripe patterns is in the non-trivial spatial direction a periodic repetition of localized pulses, traveling with a constant speed. For the Gray-Scott model, existence and stability of periodic isolated pulses was already studied in [34, 39, 36], and most of the techniques used in Chapter 5 are adapted from those articles. However, a big difference with the Gray-Scott model is the occurrence of an advection term (induced by the slope) in our model. Contrary to the Gray-Scott model, the system studied in Chapter 5 therefore does not possess a reversibility symmetry, on which the proofs in the cited articles rely heavily.

Another motivation to study specifically these types of patterns, is the numerical analysis done in [143], which shows that the stability regime of two-dimensional stripe patterns increases with the slope of the terrain. This indicates that for large enough slopes, the stripe patterns that are solutions to our model could indeed be observed in the field.

Relying on Fenichel's theorems, we first construct a single traveling, localized pulse in an infinite domain; a homoclinic traveling wave as solution of the system. This is later extended to periodic patterns with a long wavelength; the periodic extension of localized pulses. Since the validity of GSPT depends on the scale splitting of a system, a scale analysis of the model is essential and corresponds directly to the fact that the periodic patterns we construct necessarily have a long wave length. To prove the existence of periodic patterns, we cannot carry over the methods used on the Gray-Scott model, because of a lack of symmetry. Hence, a novel approach using a contraction mapping argument is used to guarantee existence of such a periodic pattern.

Lastly, the stability of both those types of traveling wave solutions to the vegetation model is analyzed using an Evans function approach as presented in [35]. Due to the scale separation of the system, the Evans function factorizes in a slow and a fast part, too. The slow component is solved using hypergeometric functions, and a full overview of the stability of periodic patterns is given. The main result is that, despite the numerical results in [143], all the constructed patterns are unstable in a two-dimensional sense. That is, perturbations in the transverse direction destabilize the striped pattern. There are several explanations for this given in the discussion of Chapter 5. Considering only one-dimensional patterns (thereby neglecting the assumed trivial extension in the other direction), there are several destabilization mechanisms possible depending on the parameters. More importantly: there are parameter regimes for which the one-dimensional patterns are stable. Although one dimension is not representing the initial application of the system, vegetation patterns, this is a valuable result in a more abstract sense.